Publication Year	2017
Acceptance in OA	2020-09-16T10:41:01Z
Title	Scientific prospects for spectroscopy of the gamma-ray burst prompt emission with SVOM
Authors	BERNARDINI, Maria Grazia, Xie, F., Sizun, P., Piron, F., Dong, Y., Atteia, J. -L., Antier, S., Daigne, F., Godet, O., Cordier, B., Wei, J.
Publisher's version (DOI)	10.1007/s10686-017-9551-4
Handle	http://hdl.handle.net/20.500.12386/27407
Journal	EXPERIMENTAL ASTRONOMY
Volume	44

Experimental Astronomy manuscript No.
(will be inserted by the editor)

Scientific prospects for spectroscopy of the gamma-ray burst prompt emission with SVOM

M. G. Bernardini · F. Xie · P. Sizun · F. Piron · Y. Dong · J.-L. Atteia · S. Antier · F. Daigne · O. Godet · B. Cordier · J. Wei

Abstract *SVOM* (Space-based multi-band astronomical Variable Objects Monitor) is a Sino-French space mission dedicated to the study of Gamma-Ray Bursts (GRBs) in the next decade, capable to detect and localise the GRB emission, and to follow its evolution in the high-energy and X-ray domains, and in the visible and NIR bands. The satellite carries two wide-field high-energy instruments: a coded-mask gamma-ray imager (ECLAIRs; 4–150 keV), and a gamma-ray spectrometer (GRM; 15–5500 keV) that, together, will characterise the GRB prompt emission spectrum over a wide

M.G. Bernardini
Laboratoire Univers et Particules de Montpellier, Université de Montpellier, CNRS/IN2P3, Montpellier, France
INAF–Osservatorio Astronomico di Brera, via E. Bianchi 46, I–23807 Merate, Italy
E-mail: bernardini@lupm.in2p3.fr

F. Piron
Laboratoire Univers et Particules de Montpellier, Université de Montpellier, CNRS/IN2P3, Montpellier, France

F. Xie
KTH Royal Institute of Technology, Roslagstullsbacken 21, 10691 Stockholm, Sweden
Key laboratory of particle and astrophysics, CAS, No. 19B Yuquan Road, 100049 Beijing, China

P. Sizun · B. Cordier
CEA Saclay, DSM/IRFU/Service d'Astrophysique, 91191 Gif-sur-Yvette, France

Y. Dong
Key laboratory of High Energy Physics, CAS, 19B Yuquan Road, 100049 Beijing, China

J.-L. Atteia · O. Godet
Université de Toulouse; UPS-OMP; IRAP; Toulouse, France
CNRS; IRAP; 14, avenue Edouard Belin, F-31400 Toulouse, France

S. Antier
LAL, Univ. Paris-Sud, CNRS/IN2P3, Université Paris-Saclay, Orsay, France
CEA Saclay, DSM/IRFU/Service d'Astrophysique, 91191 Gif-sur-Yvette, France

F. Daigne
UPMC-CNRS, UMR7095, Institut d'Astrophysique de Paris, F-75014, Paris, France

J. Wei
National Astronomical Observatories/CAS, 20A Datun Road, 100012 Beijing, China

energy range. In this paper we describe the performances of the ECLAIRs and GRM system with different populations of GRBs from existing catalogues, from the classical ones to those with a possible thermal component superimposed to their non-thermal emission. The combination of ECLAIRs and the GRM will provide new insights also on other GRB properties, as for example the spectral characterisation of the subclass of short GRBs showing an extended emission after the initial spike.

Keywords Gamma-ray burst: general · Instrumentation: detectors · Radiation mechanisms: general

1 Introduction

The observations of Gamma-Ray Bursts (GRBs) at high-energy with the Burst and Transient Source Experiment (BATSE) on board the Compton Gamma-Ray Observatory (CGRO) and the Gamma-ray Burst Monitor (GBM) and the Large Area Telescope (LAT) on board the *Fermi* satellite have revealed the complexity of their spectra in the prompt phase. The phenomenological Band function (Band et al. 1993), which consists of two smoothly connected power laws, is successful in reproducing most of the GRB observed spectra. However, spectral analyses of the *Fermi* GRB data have shown the existence of multiple components in addition to it (see e.g. Guiriec et al. 2015 and reference therein), showing the complexity of the prompt emission mechanisms.

There are also many open issues related to the prompt emission of GRBs with a single spectral component. The prompt radiation is likely related to synchrotron emission from a population of accelerated electrons, however the pure synchrotron model predictions about the low-energy spectral index are violated in a large fraction of cases (the so-called synchrotron "line of death", Katz 1994; Crider et al. 1997; Preece et al. 1998, 2002; Ghirlanda et al. 2003), as well as the observed curvature of the spectra (Yu et al. 2015). Concerning the dichotomy between short and long GRBs, it is well known that short GRBs are harder than long GRBs. However, it is still debated whether this difference arises mainly from the higher peak energy of from the harder low-energy spectral index of short GRBs (see, e.g., Ghirlanda et al. 2015 and references therein).

A better understanding of the physical origin of the prompt emission requires a sample of GRBs with well measured properties, with a good temporal resolution, a large spectral range, from the visible range to the high-energy gamma-rays, including X-rays and soft gamma-rays, and a high fraction of GRBs with redshift measurements, to constrain the GRB properties in the rest frame. *SVOM* (Space-based multi-band astronomical Variable Objects Monitor) is well designed to study the physics of the GRB phenomenon in all its diversity, thanks to an excellent spectral and temporal coverage of the prompt and afterglow emission combined with an optimised follow-up strategy aiming at the redshift determination for a large fraction of GRBs ($\sim 2/3$, Wei et al. 2016).

Specifically, the study of GRB prompt high-energy emission will benefit from the possibility to combine the data from two instruments onboard the *SVOM* satellite:

- the French ECLAIRs telescope, dedicated to observations in the hard X-ray range (4–150 keV). Detailed descriptions of ECLAIRs are provided in Godet et al. (2014); Lacombe et al. (2014); Le Provost et al. (2014); Schanne et al. (2014, 2015);
- the Chinese GRM monitor, dedicated to the observations in the gamma-ray range (15–5500 keV) thanks to its three Gamma-Ray Detectors (Wei et al. 2016). These GRDs are inclined with an angle of 30 deg with respect to the ECLAIRs pointing direction, and arranged with an azimuthal angle of 120 deg between each other, which ensures a broad sky coverage while maintaining a good overlap between their respective fields of view (half angle of $\sim$ 60 deg each).

The combination of ECLAIRs and GRM will permit to fully characterise the temporal and spectral properties of the high-energy prompt emission of all the GRBs that will be observed in common ($\sim$ 70 GRBs/yr, Wei et al. 2016). Apart from the new discovery windows that will be open on, e.g., X-ray flashes, ultra-long GRBs, etc. (Wei et al. 2016), the ECLAIRs+GRM system will represent also a step forward in the spectral characterisation of the "classical" population of long and short GRBs. In this paper we describe how the ECLAIRs and GRM joint observations will be extremely valuable to fully characterise the GRB spectral shape over a wide energy range, thanks to the ECLAIRs low-energy threshold of 4 keV, and the high sensitivity of the GRM up to MeV energies. To this aim, we tested their performances with different populations of GRBs, from the classical ones whose prompt emission is described by a Band function, to the ones with a possible thermal component superimposed to their non-thermal emission. The combination of ECLAIRs and the GRM will provide new insights also on other properties of the GRB class, as for example the spectral characterisation of the subclass of short GRBs showing a soft extended emission after the initial hard spike (Norris & Bonnell 2006).

In Section 2 we describe the methodology we used to simulate and analyse different populations of GRBs with the *SVOM*/ECLAIRs+GRM system and the *Fermi*/GBM instrument. In Section 3 we compare the spectroscopic performances of ECLAIRs+GRM and the *Fermi*/GBM in the keV–MeV range, based on simulations of the *Fermi*/GBM spectral catalogue. We discuss the prospects for the spectroscopy of bright GRBs with a thermal component in Section 4 and for short GRBs with and extended emission in Section 5. We present our conclusions in Section 6. Errors are given at 1σ confidence level, unless otherwise stated.

2 Methodology

In this work all the simulated sources are on-axis with respect to the *SVOM* spacecraft, i. e. the angle between the source position and the optical axis is 0 deg for ECLAIRs and 30 deg for the GRDs. For this configuration that is the most favourable for SVOM, we simulated the spectral response files of both ECLAIRs and each of the three GRDs with the Geant4[1] toolkit, with a detailed model of each instrument. The resulting total effective areas are portrayed in fig. 1.

[1] http://geant4.cern.ch/

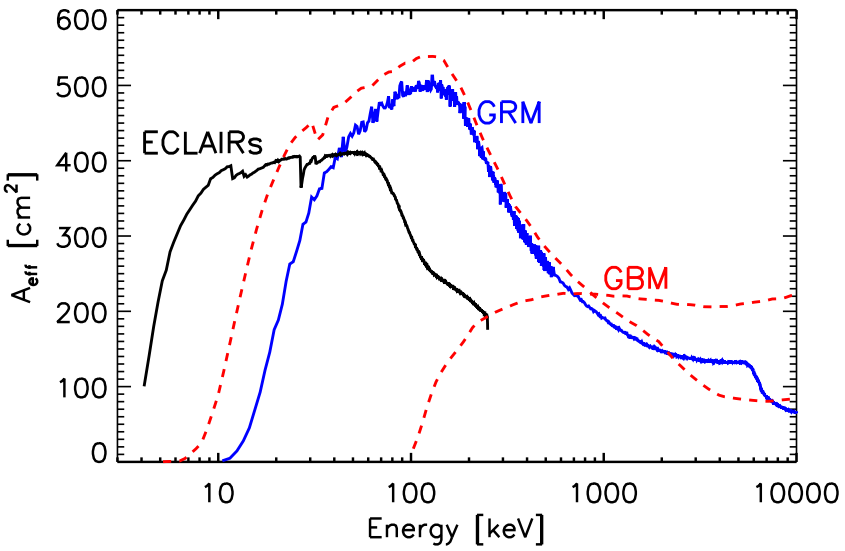

Fig. 1 Total effective area of ECLAIRs for on-axis sources (black line) and of the GRM for sources located 30 deg off-axis (blue line) simulated with the Gean4 toolkit. The red dashed lines mark the effective area for the *Fermi*/GBM corresponding to four NaI and one BGO detectors.

We used the same setup to simulate the average background for each instrument with the Geant4 toolkit (Godet et al. 2009; Zhao et al. 2012). Since the major contribution at low energies comes from the cosmic X-ray background (CXB), for ECLAIRs we modelled the background with the CXB spectral model from Moretti et al. (2009) below 164 keV and of Gruber et al. (1999) above. For the GRM, we used a spectral model that includes also the contributions from the Earth's albedo (Churazov et al. 2006), the cosmic ray-induced radiation from the Earth's atmosphere (Sazonov et al. 2007), the activation after each passage inside the SAA, that is the dominant component at high energies. The CXB component depends the most on the Earth position with respect to the spacecraft, and is minimum when the Earth is in front of the spacecraft. In order to account entirely for the background, we performed the simulations assuming that the Earth is behind the spacecraft, which corresponds to the maximum background from the CXB. The background used for the two instruments is portrayed in fig. 2.

The background and spectral response files have been used to evaluate the performances of the two instruments in this configuration in detecting different features of the GRB prompt emission spectrum. For this purpose, we made use of the XSPEC (v.12.9) command FAKEIT to simulate synthetic spectra: assuming an analytical model to describe the spectrum, we ran the FAKEIT with the background and response files for ECLAIRs and the three GRDs. We finally fitted within XSPEC the simulated spectra with different combinations of the following analytical functions:

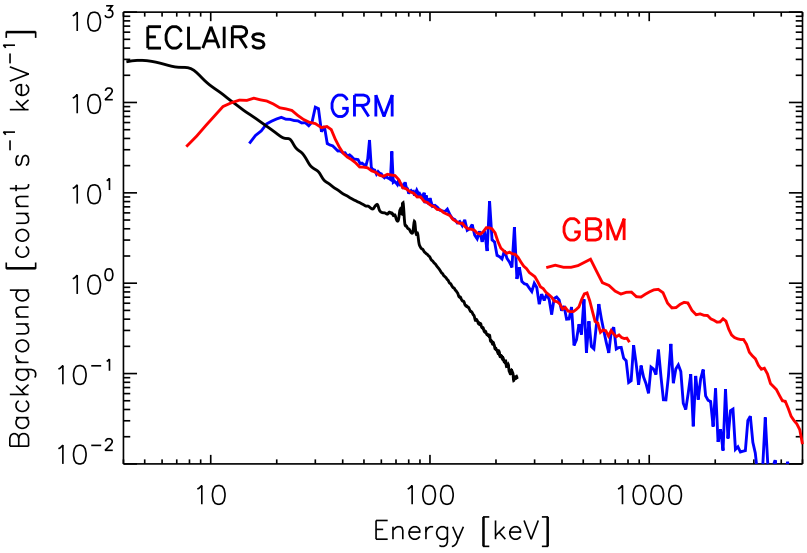

Fig. 2 Simulated background for ECLAIRs (black line) and the GRM (blue line). The red line marks the observed background for the *Fermi*/GBM corresponding to four NaI and one BGO detectors.

power-law (PL), power-law with an exponential cutoff (cutPL), smoothly-joined broken power law (Band) and black body (BB). The definition of these functions is given in Appendix A. We used the Cstat as fitting statistics, and for the model hypothesis testing we used a confidence level of 3σ.

We chose the *Fermi*/GBM (Meegan et al. 2009) as a reference to assess the performances of the ECLAIRs+GRM system. The *Fermi*/GBM is composed of two types of detectors that cover a wider energy range at high energies than ECLAIRs and the GRM: 12 NaI (8 – 1000 keV) and 2 BGO (0.2 – 40 MeV). In order to perform a fair comparison, instead of using the results from the spectral fitting of real sources observed by the *Fermi*/GBM, we simulated and analysed synthetic spectra with the same procedure used for the ECLAIRs+GRM system, using the observed response files for the NaI and BGO detectors. The NaI detectors are located and oriented differently in the spacecraft, so that they are not all fully illuminated by a source at a time. Since the aim of this work is to provide a quantitative comparison to evaluate the performances of the ECLAIRs+GRM system, we considered for the *Fermi*/GBM a setup that is equivalent in terms of the effective area. This corresponds to use four NaI and one BGO detectors in the simulations, so that the overall effective area is comparable to that of three GRDs over the entire energy range where they overlap (see fig. 1). For the *Fermi*/GBM, we used a measured background on orbit (see e.g. Meegan et al. 2009). When compared to the simulated background for ECLAIRs+GRM, they result to be consistent (see fig. 2), ensuring that the comparison on the derived spectral parameters is not biased by a systematic difference in the background.

3 GRBs with a single spectral component

In order to test the performances of ECLAIRs and the GRM for the spectroscopy of GRBs, we simulated the spectral properties of the population of GRBs observed by the *Fermi*/GBM. We made use of the *Fermi*/GBM spectral catalogue (Gruber et al. 2014), that comprises the best-fitting models for the time-integrated prompt emission spectra of 943 triggered GRBs. We restricted our analysis to the 446 GRBs whose spectrum is described by a cutPL function and the 75 GRBs by a Band function[2]. For all these GRBs, we simulated the prompt emission spectra as observed by the ECLAIRs+GRM system with the procedure described in section 2, and we fitted all the simulated spectra with both the cutPL and the Band functions.

Concerning the population of GRBs characterised by a Band spectrum, we find that the best-fitting model is the one used to create the simulated spectrum in 96% of cases (73/75), indicating that the spectral coverage of the ECLAIRs+GRM system is sufficient to discriminate between the two models and to constrain the high-energy spectral index. For both spectral models, we always find consistency within the errors between the best-fitting spectral parameters and the values adopted in the simulations (see fig. 3).

The uncertainties on the spectral parameters are also very well constrained using ECLAIRs+GRM. For the low-energy spectral indices α, the medians of the distributions of the 1σ confidence interval are $\overline{\sigma(\alpha)} = 0.05$ and 0.02 for the cutPL and the Band models, respectively. For the characteristic energies, we find that the median of the relative error on the characteristic energy $\delta E_\circ = \sigma(E_\circ)/E_\circ$ is $\overline{\delta \mathrm{E}_\circ} = 0.14$ and 0.07 for the cutPL and the Band models, respectively.

We compared these results with the ones obtained from the *Fermi*/GBM using the same simulation procedure, as described in section 2. Even if the *Fermi*/GBM has a broader energy range at high energies thanks to the BGO detector, the correct model used to simulate the data is retrieved only in 82% of cases. In addition, the uncertainties on the spectral parameters measured with ECLAIRs+GRM are usually smaller than those derived with *Fermi*/GBM. In fig. 4 we compare the 1σ confidence interval of the different spectral parameters for the cutPL and Band models obtained with ECLAIRs+GRM and with the *Fermi*/GBM. For the low energy spectral index, the uncertainties are always smaller with the ECLAIRs+GRM system. The median value of the ratio between the 1σ error on α obtained with the *Fermi*/GBM and with ECLAIRs+GRM is 2.4 and 2.9 for the cutPL and the Band models, respectively. For the characteristic energies, the fraction of smaller uncertainties is 90% and 100% for the cutPL and the Band models, respectively, with a median of the 1σ error ratio 1.5 and 2.4 for the cutPL and the Band models, respectively. Regarding the high-energy spectral index of the Band function, the *Fermi*/GBM may take advantage from its broader energy range. However, we obtained similar errors between the *Fermi*/GBM and ECLAIRs+GRM, with a median of the 1σ error ratio equal to one.

Using the condition for the duration $\leqslant$ 2 s, there are 52 short GRBs in the sample that we considered: 50 GRBs belong to the simulated cutPL sample and 2 to the simulated Band sample. For the 50 spectra fitted with the cutPL model, we found that

[2] We recall that the cutPL function is a subset of the Band function, obtained in the limit $\beta \to \infty$.

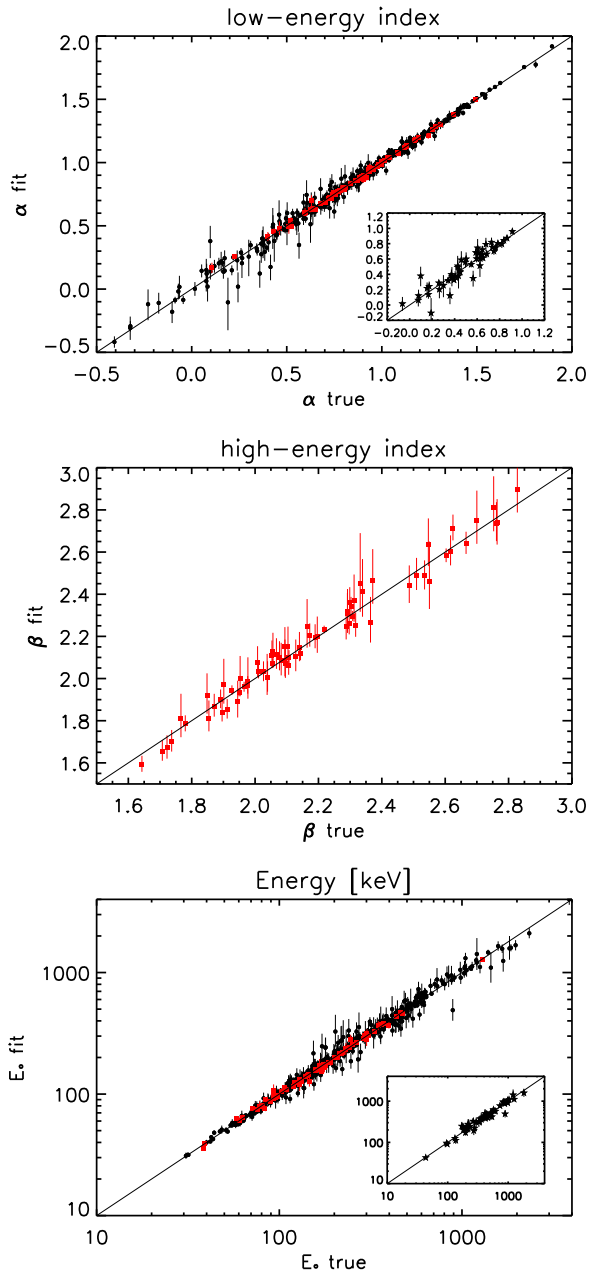

Fig. 3 Best-fitting spectral parameters (low-energy spectral index α, upper panel, high-energy spectral index β, middle panel, and characteristic energy $E_\circ$, lower panel) for the cutPL (black points, 446 GRBs) and Band (red squares, 73 GRBs) functions, compared to the "true" values used to simulate the spectra with the ECLAIRs+GRM system. The solid lines mark the equality. The same quantities for the 50 short GRBs are portrayed in the insets.

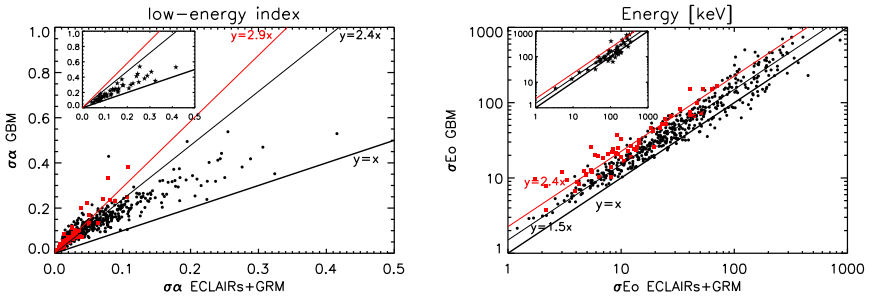

Fig. 4 90% confidence interval on the best-fitting spectral parameters (low-energy spectral index α, left panel, and characteristic energy $E_\circ$, right panel) for the cutPL (black points, 446 GRBs) and Band (red squares, 58 GRBs whose best fit is a Band function for both ECLAIRs+GRM and *Fermi*/GBM) functions obtained with the ECLAIRs+GRM system versus those obtained with the *Fermi*/GBM. The 50 short GRBs are marked with a star. The solid thick lines mark the equality, while the solid thin lines mark the median relation. The same quantities for the 50 short GRBs are portrayed in the insets.

the uncertainties on the low-energy spectral index are always smaller with the the ECLAIRs+GRM system, with a median of the 1σ error ratio 1.6. For the characteristic energies, the fraction of smaller uncertainties is 74%, with a median of the 1σ error ratio 1.4. The 2 bursts belonging to the simulated Band sample are those where the cutPL model is preferred to the Band model in the fitting procedure.

Figure 3 shows that the errors on the characteristic energies are smaller below $\sim$ 200 keV, which obviously comes from the ECLAIRs contribution to the spectral reconstruction. In addition, ECLAIRs helps to constrain the spectral parameters at higher energies. If we perform the spectral analysis of the data from the GRM only and we compare the results with those obtained for the ECLAIRs+GRM system, we find that the errors on, e.g., the characteristic energy of the cutPL model $E_\circ$ are on average 1.3 times larger for the GRM alone even when we consider only the cases with $E_\circ > 1000$ keV. In addition, the results obtained for the GRM alone are fully consistent with those obtained for the *Fermi*/GBM in all ranges. This simple test shows that while the GRM is essential to constrain the spectral model and to measure the peak energy, ECLAIRs provides a fundamental contribution to constrain the spectral parameters and represents the major improvement for spectroscopy with respect to the *Fermi*/GBM.

We finally tested how these performances depend on the inter-calibration between ECLAIRs and the GRM. We repeated the simulations of the GRB sample, adding a random systematic error in the flux measurement between ECLAIRs and the GRM. In practice, we left the simulated flux unchanged for ECLAIRs, while we multiplied it for each GRD by a factor that was drawn from a gaussian distribution centred on unity and with a 10% standard deviation. In this situation the correct model used to simulate the data is retrieved only in 74% of cases. However, for these cases, the determination of the spectral parameters and their uncertainties are not affected significantly.

The figures that we derived depend on the specific configuration of the instruments that we adopted in the simulations, with the purpose to illustrate the perfor-

Table 1 Parameters used to simulate the prompt emission time-integrated spectrum of GRB 100724B from Guiriec et al. (2011) (the integration time is 84.9 s) and best-fitting parameters for the tested models.

model	α	β	$E_\circ$ (keV)	kT (keV)	Cstat/dof
Band+BB	0.9	2.1	512.0	38.0	–
cutPL	0.785 ± 0.003	–	382 ± 4	–	9275/6619
Band	0.728 ± 0.04	2.04 ± 0.01	289 ± 3.8	–	7498/6618
cutPL+BB	0.995 ± 0.005	–	897^{+28}_{-25}	37.1 ± 0.3	7655/6617
Band+BB	0.903 ± 0.008	2.10 ± 0.02	517^{+19}_{-18}	38.1 ± 0.5	6996/6616

mance of the ECLAIRs+GRM system. Indeed, for off-axis sources, the effective area of ECLAIRs is reduced, while *Fermi*/GBM has an even coverage of the sky. However, the configuration we adopted for *Fermi*/GBM is among the most favourable (Connaughton, private communication), indicating that the ECLAIRs+GRM system will provide a valuable contribution for GRB prompt emission spectroscopy.

4 Multiple components in the prompt emission spectrum

The important role of ECLAIRs in supporting the GRM for GRB spectroscopy is even more evident when we consider the prompt emission spectrum of other populations of "classical" GRBs, not described by a single component. The analysis of the prompt emission spectrum of bright GRBs observed by the *Fermi*/GBM revealed the presence of a possible black-body component superimposed to the non-thermal spectrum in a number of cases, peaking around 100 keV (see e.g. Guiriec et al. 2011). Though these GRBs may not be representative of the population of GRBs observed by the *Fermi*/GBM, their identification is highly constraining for the emission mechanisms involved in the prompt emission. In addition, the correct modelling of the prompt emission is necessary to constrain better the parameters of the non-thermal component, whose estimate may be affected by this hidden extra-component.

We selected GRB 100724B, a long GRB (T_{90} = 84.9 s) that is one of the brightest GRBs observed by the *Fermi*/GBM, as a test case to illustrate how the ECLAIRs+GRM system can contribute to this topic. The time-integrated spectrum of GRB 100724B in the 8 keV−40 MeV energy band is best described by a Band function with the addition of a black-body component, that comprises 10% of the total flux in the energy range 10 − 1000 keV (Guiriec et al. 2011). We simulated this spectral model using the Band+BB model as described in section 2. Then we fitted the simulated spectrum with different models (see tab. 1), finding that the Band function with the addition of a BB component provides the best representation of the data, and the best-fitting parameters are consistent with the values injected in the simulated (see tab. 1). In addition, the non-identification of the BB component leads to an underestimate of the peak energy of the spectrum, as also pointed out by Guiriec et al. (2011), as well as a significantly different low-energy spectral index. The unfolded energy density spectrum EF(E) with best-fitting model is displayed in fig. 5.

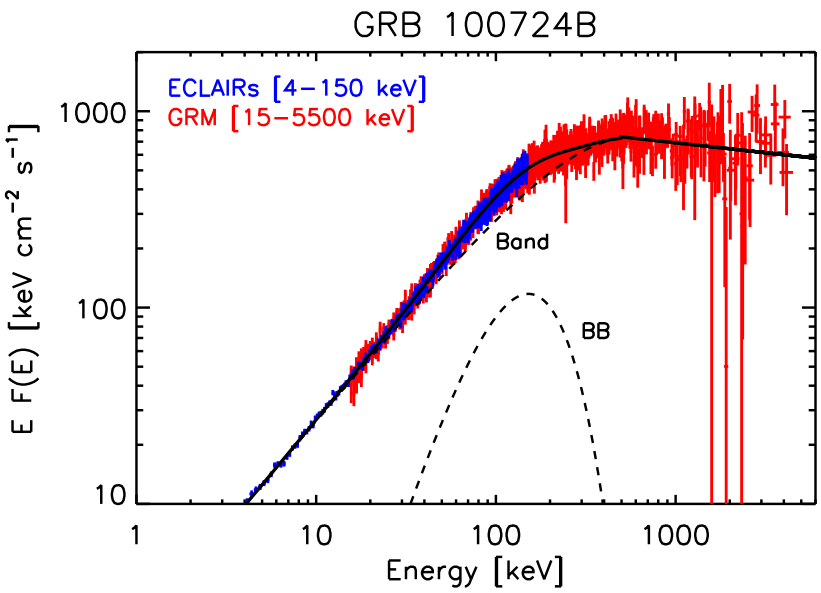

Fig. 5 Simulated energy density spectrum of GRB 100724B for ECLAIRs and the GRM with the best-fitting model Band+BB (solid line) and the two spectral components (dashed lines).

In order to explore the sensitivity of the ECLAIRs+GRM system to the thermal component, we used a Band function with the spectral parameters of GRB 100724B as a prototype, and we varied the black-body temperature (40 and 100 keV) and its flux in the energy range 10−1000 keV (1%, 5% and 10% of the total flux). Since GRB 100724B is bright (average flux $f_{tot} = 2.6 \times 10^{-6}$ erg cm^{-2} s $^{-1}$), we also tested the capabilities of retrieving the black-body component if the GRB total flux is 10% and 50% of the one observed in GRB 100724B, without changing the spectral parameters. In fig. 6 we summarise our results in terms of the ΔCstat obtained with the addition of the BB component compared to the fit with the simple Band function.

We find that the addition of a black-body component is never statistically required when the flux of the BB component is 1% of the total one, regardless of the total flux, and for the lowest total flux. On the contrary, it is correctly retrieved in all the other cases for a black-body temperature $T_{BB} = 40$ keV, i.e. in the region where the energy ranges of ECLAIRs and GRM overlap, and the best-fitting parameters are consistent with the injected ones. For $T_{BB} = 100$ keV, i.e. for a peak energy of the BB component within the energy range of GRM alone and closer to the peak of the Band spectrum, the BB component is retrieved only for the brighter cases.

5 Short GRBs with extended emission

We finally discuss some prospects for the spectroscopy with ECLAIRs and the GRM of a special class of short GRBs, which exhibit a long-lasting tail in the prompt emis-

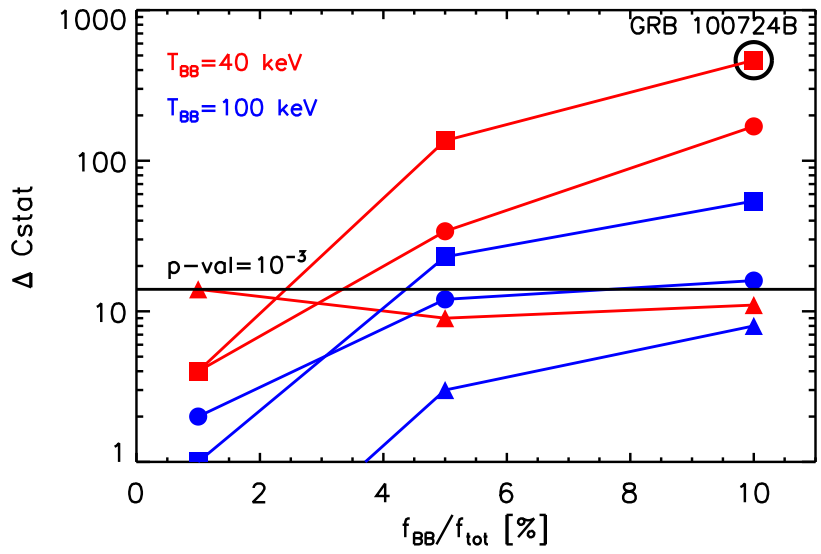

Fig. 6 ΔCstat obtained with the addition of the BB component compared to the fit with the simple Band function versus the ratio of the black-body flux over the total flux, for a total flux $f_{tot} = 2.6 \times 10^{-7}$ erg cm^{-2} s^{-1} (triangles), $f_{tot} = 1.3 \times 10^{-6}$ erg cm^{-2} s^{-1} (circles) and $f_{tot} = 2.6 \times 10^{-6}$ erg cm^{-2} s^{-1} (squares), and for $T_{BB} = 40$ keV (red) and $T_{BB} = 100$ keV (blue). The black solid line marks the ΔCstat that corresponds to a 3σ confidence interval for two degrees of freedom. The case corresponding to GRB 100724B is marked with a black circle.

sion after the initial spike. These short GRBs were first discovered in the BATSE sample (Lazzati et al. 2001; Norris & Bonnell 2006) and then confirmed with HETE II and *Swift* (e.g., Villasenor et al. 2005; Barthelmy et al. 2005), and they represent ∼ 15% of the population of short GRBs. This extended emission (EE) is long-lasting, up to ∼ 100 s, its onset is usually delayed from the initial spike and it is characterised by a softer spectrum compared to the initial spike and to long GRBs of similar duration (see D'Avanzo 2015 for a recent review).

The observation of short GRBs with EE will clearly benefit from the synergy between ECLAIRs and the GRM to characterise simultaneously both the initial (hard) spike and the following (soft) tail. Joint simulations with ECLAIRs and the GRM have been performed to determine the detection performance for GRB 990712A, observed by BATSE, as a test case (see Wei et al. 2016). The hard peak preferentially triggers the GRM whereas the X-ray rich soft tail triggers ECLAIRs. Overall, the combined ECLAIRs+GRM trigger could help the decision of the slew of the satellite and follow-up observations in X-ray energy band and optical domain. A complete discussion of the detection performances of *SVOM* for the class of short GRBs is beyond the scope of the present paper and it will be presented elsewhere. Here we will outline the capability of the ECLAIRs+GRM system in constraining the spectral properties of short GRBs with an EE.

Table 2 Parameters used to simulate the spectrum of the initial spike and of the EE of GRB 990712A from Kaneko et al. (2006), and the parameters for the best fitting model for each instrument separately and for the ECLAIRs+GRM system.

instrument	model	α	$E_\circ$ (keV)
Initial spike			
	cutPL	0.23	627
ECLAIRs	PL	0.34 ± 0.05	–
GRM	cutPL	0.15 ± 0.05	593^{+48}_{-44}
ECLAIRs+GRM	cutPL	0.22 ± 0.03	635^{+45}_{-41}
Extended Emission			
	PL	1.93	–
ECLAIRs	PL	1.94 ± 0.01	–
GRM	PL	1.97 ± 0.04	–
ECLAIRs+GRM	PL	1.94 ± 0.01	–

We made use of the time-resolved spectral analysis of GRB 990712A in the range 30 – 1800 keV reported in the spectral catalog of BATSE bright GRBs (Kaneko et al. 2006). We simulated the spectra of different time intervals using the corresponding models as described in section 2 (see tab. 2). Then we fitted the simulated spectra with different functions in XSPEC (PL and cutPL) for ECLAIRs and GRM separately, and for the ECLAIRs+GRM system. The results for the peak of the initial spike and the EE time intervals are reported in tab. 2 and illustrated in fig. 7.

The spectral analysis of both the initial spike and of the extended emission clearly benefits from the combination of the two instruments. For the initial spike, ECLAIRs alone is capable to constrain only the spectral slope, with the PL model being statistically preferred than the cutPL model, while the GRM alone is sufficient to determine the injected spectral model, and is able to constrain the cutoff energy. However, with the combination of the two instruments we are able to estimate with better precision both these spectral parameters, as also shown in section 3.

6 Conclusions

In this paper we tested the performances of ECLAIRs and the GRM joint spectroscopy of GRB prompt emission using the population of GRBs observed by the *Fermi*/GBM, and we explored also their capability in detecting a possible thermal component superimposed to the non-thermal spectrum. Finally, we discussed some prospects for the spectroscopy of the subclass of short GRBs with an extended emission.

This analysis shows how this system will be extremely valuable to fully characterise the GRB spectral properties. For the GRBs in the common field of view, the GRM will be able to constrain the spectral model and to measure the peak energy, while ECLAIRs provides a fundamental contribution to constrain the spectral parameters especially in presence of a possible thermal component peaking below

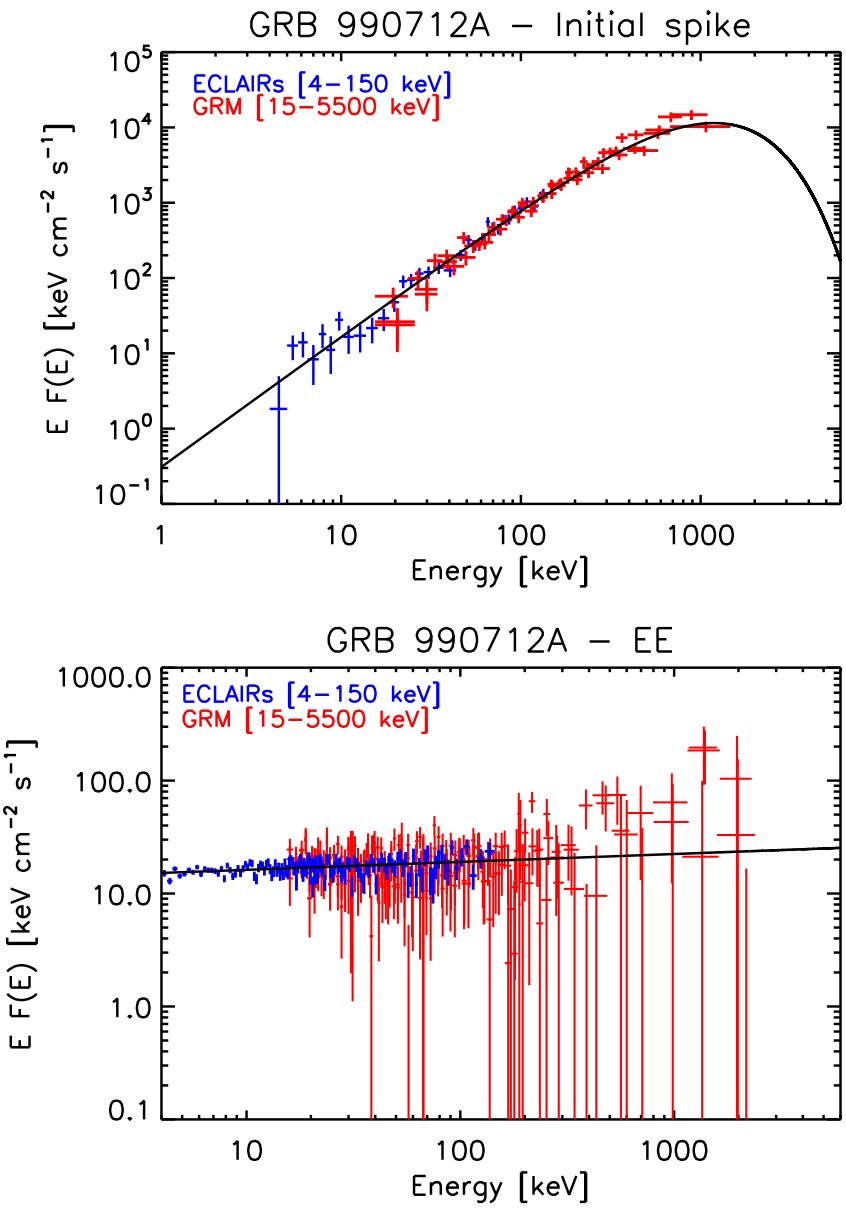

Fig. 7 Simulated energy density spectrum of GRB 990712A for ECLAIRs and the GRM with the best-fitting model for the peak of the initial spike (upper panel) and the EE (lower panel) time interval.

100 keV, representing the major improvement for spectroscopy with respect to the *Fermi*/GBM. In addition, the *SVOM* optimised follow-up strategy for the redshift determination will permit to build a sample of GRBs with well-measured spectral properties to be used to investigate the nature of the prompt emission spectrum and to test the different kind of correlations involving prompt emission quantities (Amati et al. 2002; Ghirlanda et al. 2004; Yonetoku et al. 2004, see e.g. Heussaff et al. 2013). This represents an improvement with respect to the current situation where most of the GRBs with redshift measurement are detected by *Swift*, with a narrower energy coverage in the prompt emission.

Acknowledgements

We thank the anonymous referee for the valuable comments and suggestions. This work has been carried out thanks to the support of the OCEVU Labex (ANR-11-LABX-0060) and the A*MIDEX project (ANR-11-IDEX-0001-02) funded by the "Investissements d'Avenir" French government program managed by the ANR. YWD acknowledges the Youth Innovation Promotion Association CAS under Grant NO. 2014009.

References

Amati, L., Frontera, F., Tavani, M., et al. 2002, Astron. Astrophys., 390, 81
Band, D., Matteson, J., Ford, L., et al. 1993, Astrophys. J., 413, 281
Barthelmy, S. D., Chincarini, G., Burrows, D. N., et al. 2005, Nature, 438, 994
Churazov, E., Sazonov, S., Sunyaev, R., & Revnivtsev, M. 2006, ArXiv astro-ph/0608252
Crider, A., Liang, E. P., Smith, I. A., et al. 1997, Astrophys. J. Lett., 479, L39
D'Avanzo, P. 2015, Journal of High Energy Astrophysics, 7, 73
Ghirlanda, G., Bernardini, M. G., Calderone, G., & D'Avanzo, P. 2015, Journal of High Energy Astrophysics, 7, 81
Ghirlanda, G., Celotti, A., & Ghisellini, G. 2003, Astron. Astrophys., 406, 879
Ghirlanda, G., Ghisellini, G., & Lazzati, D. 2004, Astrophys. J., 616, 331
Godet, O., Nasser, G., Atteia, J.-., et al. 2014, in Proceedings of the SPIE, Vol. 9144, Space Telescopes and Instrumentation 2014: Ultraviolet to Gamma Ray, 914424
Godet, O., Sizun, P., Barret, D., et al. 2009, Nuclear Instruments and Methods in Physics Research A, 603, 365
Gruber, D., Goldstein, A., Weller von Ahlefeld, V., et al. 2014, Astrophys. J. Supp. Series, 211, 12
Gruber, D. E., Matteson, J. L., Peterson, L. E., & Jung, G. V. 1999, Astrophys. J., 520, 124
Guiriec, S., Connaughton, V., Briggs, M. S., et al. 2011, Astrophys. J. Lett., 727, L33
Guiriec, S., Kouveliotou, C., Daigne, F., et al. 2015, Astrophys. J., 807, 148
Heussaff, V., Atteia, J.-L., & Zolnierowski, Y. 2013, Astron. Astrophys., 557, A100
Kaneko, Y., Preece, R. D., Briggs, M. S., et al. 2006, Astrophys. J. Supp. Series, 166, 298

Katz, J. I. 1994, Astrophys. J. Lett., 432, L107
Lacombe, K., Pons, R., Amoros, C., et al. 2014, in Proceedings of the SPIE, Vol. 9144, Space Telescopes and Instrumentation 2014: Ultraviolet to Gamma Ray, 914451
Lazzati, D., Ramirez-Ruiz, E., & Ghisellini, G. 2001, Astron. Astrophys., 379, L39
Le Provost, H., Schanne, S., Flouzat, C., et al. 2014, ArXiv 1412.0481
Meegan, C., Lichti, G., Bhat, P. N., et al. 2009, Astrophys. J., 702, 791
Moretti, A., Pagani, C., Cusumano, G., et al. 2009, Astron. Astrophys., 493, 501
Norris, J. P. & Bonnell, J. T. 2006, Astrophys. J., 643, 266
Preece, R. D., Briggs, M. S., Giblin, T. W., et al. 2002, Astrophys. J., 581, 1248
Preece, R. D., Briggs, M. S., Mallozzi, R. S., et al. 1998, Astrophys. J. Lett., 506, L23
Sazonov, S., Churazov, E., Sunyaev, R., & Revnivtsev, M. 2007, MNRAS, 377, 1726
Schanne, S., Cordier, B., Atteia, J.-L., et al. 2015, ArXiv 1508.05851
Schanne, S., Le Provost, H., Kestener, P., et al. 2014, ArXiv 1411.7810
Villasenor, J. S., Lamb, D. Q., Ricker, G. R., et al. 2005, Nature, 437, 855
Wei, J., Cordier, B., Antier, S., et al. 2016, ArXiv:1610.06892
Yonetoku, D., Murakami, T., Nakamura, T., et al. 2004, Astrophys. J., 609, 935
Yu, H.-F., van Eerten, H. J., Greiner, J., et al. 2015, Astron. Astrophys., 583, A129
Zhao, D., Cordier, B., Sizun, P., et al. 2012, Experimental Astronomy, 34, 705

A Spectral models used in the analysis

– **Power-law model (PL):**

$$\mathrm{N(E)} = \mathrm{K}\mathrm{E}^{-\alpha} \tag{1}$$

K= normalization [ph cm^{-2} s^{-1} keV^{-1} at 1 keV], α= photon index.

– **Comptonised model (cutPL):**

$$\mathrm{N(E)} = \mathrm{K}\mathrm{E}^{-\alpha}\mathrm{e}^{\left(-\frac{\mathrm{E}}{\mathrm{E}_\circ}\right)} \tag{2}$$

K= normalization [ph cm^{-2} s^{-1} keV^{-1} at 1 keV], α= photon index, $E_\circ$= e-folding energy [keV].

– **Band model (Band):**

$$\mathrm{N(E)} = \mathrm{K}\begin{cases} \left(\frac{\mathrm{E}}{100\mathrm{keV}}\right)^{-\alpha}\mathrm{e}^{\left(-\frac{\mathrm{E}}{\mathrm{E}_\circ}\right)} & \mathrm{E} \leqslant \mathrm{E}_{\mathrm{br}} \\ \left[\frac{\mathrm{E}_{\mathrm{br}}}{100\mathrm{keV}}\right]^{(\beta-\alpha)}\left(\frac{\mathrm{E}}{100\mathrm{keV}}\right)^{-\beta}\mathrm{e}^{-(\beta-\alpha)} & \mathrm{E} > \mathrm{E}_{\mathrm{br}} \end{cases} \tag{3}$$

K= normalization [ph cm^{-2} s^{-1} keV^{-1}], α= low-energy photon index, β= high-energy photon index, $E_\circ$= e-folding energy [keV], $\mathrm{E_{br}} = (\beta - \alpha)\mathrm{E}_\circ$. The cutPL function is a subset of the Band function, obtained in the limit $\beta \to \infty$.

– **Black-body model (BB):**

$$\mathrm{N(E)} = \mathrm{K}\frac{\mathrm{E}^2}{(\mathrm{kT})^4\left[\exp(\mathrm{E}/(\mathrm{kT})) - 1\right]} \tag{4}$$

K= normalization [ph keV cm^{-2} s^{-1}], kT= temperature [keV].